CoGa2O4 Nanoparticles and Films Using a Single Molecular Source

Sanjay Mathur, Christian Cavelius, Hao Shen

Zeitschrift für Anorganische und Allgemeine Chemie

CoGa2O4 Nanoparticles and Films Using a Single Molecular Source

Journal:	*Zeitschrift für Anorganische und Allgemeine Chemie*
Manuscript ID:	zaac.200900167.R2
Wiley - Manuscript type:	Research Report
Date Submitted by the Author:	22-May-2009
Complete List of Authors:	Mathur, Sanjay; Institute of Inorganic Chemistry Cavelius, Christian; Institute of New Materials Shen, Hao; Institute of Inorganic Chemistry
Keywords:	Molecular precursor, Nanoparticles and films

$CoGa_2O_4$ Nanoparticles and Films Using a Single Molecular Source[†]

Sanjay Mathur,* Christian Cavelius[†] and Hao Shen

Chair, Inorganic and Materials Chemistry
Institute of Inorganic Chemistry, University of Cologne, D-50939 Cologne, Germany

[†]*Leibniz Institute of New Materials, D-66123 Saarbruecken, Germany*

[†]*Dedicated to Prof. Dr. Michael Veith on his 65th birthday for his pioneering contributions to molecule and materials chemistry of main group elements.*

* Corresponding Author: Prof. Dr. Sanjay Mathur
Institute of Inorganic Chemistry
University of Cologne
D-50939, Cologne
Germany

Tel: +49-221-470-4107
Fax: +49-221-470-4899
E-mail: sanjay.mathur@uni-koeln.de

TOC

$CoGa_2O_4$ Nanoparticles and Films Using a Single Molecular Source

Sanjay Mathur, Christian Cavelius and Hao Shen

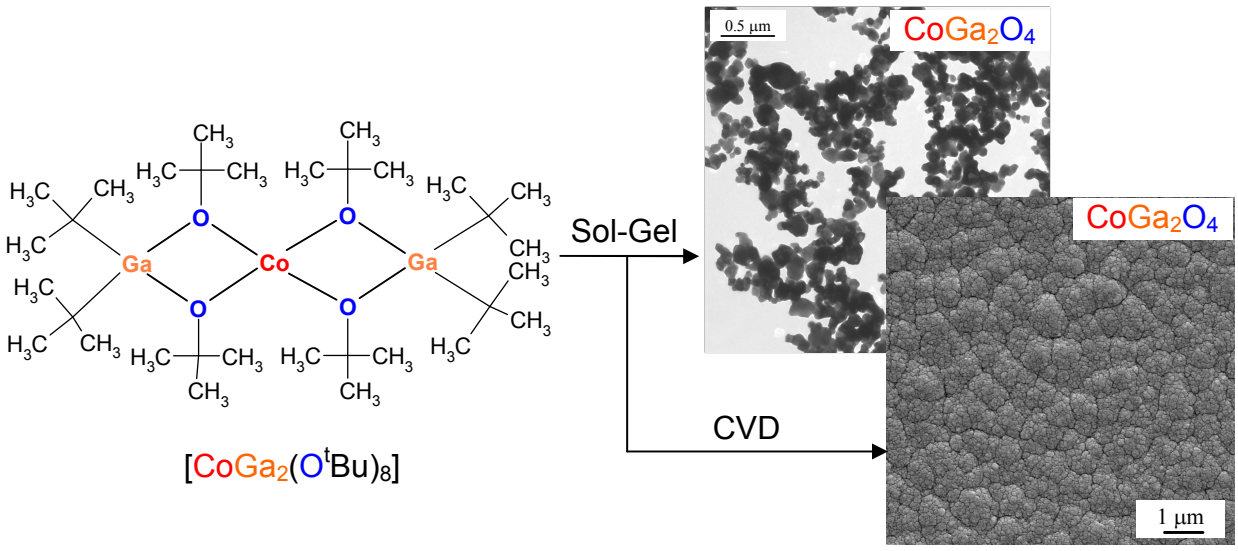

Mixed-metal *tert*-butoxide, $[CoGa_2(O^tBu)_8]$, was used in chemical vapor deposition (CVD) and sol-gel processes to obtain monophasic cobalt gallate ($CoGa_2O_4$) in film and nanoparticulate forms. The results demonstrate that the heteronuclear precursor effectively transforms at relatively low temperature (CVD: < 500 °C; Sol-Gel: < 700 °C) into nanosized $CoGa_2O_4$, without showing any micro-phase separation into individual metal oxides commonly observed in spinel produced from a mixture of individual metal sources.

Abstract

Mixed-metal *tert*-butoxide, $[CoGa_2(O^tBu)_8]$, was employed in the chemical vapor deposition (CVD) and sol-gel processes to obtain thin films and nanoparticles of spinel $CoGa_2O_4$ phase, respectively. The appropriate Co:Ga ratio and intact vaporisation (115-120 ^oC / 10^{-2} Torr) of the molecular source produced crystalline deposits of $CoGa_2O_4$ at relatively low temperatures (~ 500 ^oC). A clean transformation of the heterometal precursor in spinel oxide of definite composition was supported by TG/DTA analysis that showed no weight loss above 470 ^oC. The SEM images of $CoGa_2O_4$ films showed homogeneous morphology and dense microstructure constituted by nanometric grains (<d>, ~ 35 nm). Hydrolytic decomposition of the precursor produced gels that upon heat-treatment (400 - 1200 ^oC) formed nanoscaled spinel. For comparison, $CoGa_2O_4$ was also prepared by complexing Co^{2+} and Ga^{3+} ions with glycolate ligands, significant agglomeration effect, broader size dispersion and amorphous domains were observed indicating that low-temperature synthesis of monophasic materials following conventional chemical approaches is hampered by thermodynamic impediments. The UV-Vis spectra of $CoGa_2O_4$ particles exhibit characteristic peaks corresponding to $^4A_2(F) \rightarrow {}^4T_1(P)$ transition in the divalent cobalt cation. The magnetization data of the $CoGa_2O_4$ nanoparticles showed as expected an antiferromagentic behaviour.

Introduction

Nano-sized metal oxides in particle and film forms are gaining significant attention due to size-dependent novel mechanical, electrical, optical and magnetic properties,[1-8] which can be tuned by controlling the grain size.[9-11] For example, magnetic phases like Fe_3O_4 become superparamagnetic when the particle size is less than the critical size of Weiss domains.[12] Due to the pre-existent metal-ligand connectivity in the metal-organic compounds, they are been increasingly used as "molecular seeds" to grow nanoscopic materials.[13-15] This concept is especially attractive for materials where several phases of similar chemical composition coexist in a narrow temperature range. Although molecule-to-material transformation processes are not well-studied, the compelitive edge of molecule-based synthesis is sufficient by homogeneous chemical compositions and more importantly the ability to synthesize metastable phases. Among transition metal ternary oxides, metal gallates are promising materials for optical[16-18] and catalytic applications.[19] $CoGa_2O_4$ spinel is mainly used as oxidic semiconductor as well as color pigment. Additionally, a spin-glass behaviour is observed (T_{sg} ~ 10 K) in $CoGa_2O_4$ due to the competition between ferromagnetic and antiferromagnetic interactions.[20,21] Since the magnetic property is dependent on the nature of cobalt ions, namely, charges and charge distribution among the tetrahedral and octahedral sites, it is important to control the coordination of cobalt ions in the synthesis of $CoGa_2O_4$ spinel. Herein we report, the synthesis and characterisation of a Co-Ga mixed-metal alkoxide, $[CoGa_2(OBu^t)_8]$, and its application to grow nanostructured $CoGa_2O_4$ phase.

Experimental

Synthesis of $[CoGa_2(O^tBu)_8]$

The synthesis of mixed metal alkoxide was performed in a modified Schlenk type vacuum assembly, taking stringent precautions against atmospheric moisture.[22] Solvents were purified by standard methods and stored over appropriate desiccating agents. The hetero-bimetallic

precursor, $[CoGa_2(OBu^t)_8]$, was obtained by a salt-elimination reaction between anhydrous cobalt chloride and sodium *tetra*-alkoxogallate (eq. 1) as described by Singh and Mehrotra.[19]

$$\mathbf{CoCl_2 + 2/n\ [NaGa(O^tBu)_4]_n \rightarrow [CoGa_2(O^tBu)_8] + 2\ NaCl\downarrow} \quad (1)$$

Sol-Gel Synthesis

The sol-gel processing of the heterometal precursor proceeds via partial hydrolysis (activation) and condensation reactions. Typically, $[CoGa_2(O^tBu)_8]$ (1.351 g, 1.726 mmol) was dissolved in hot (60 °C) isopropyl alcohol and carefully hydrolyzed by adding a solution of water (0.249 g, 13.8 mmol) in isopropyl alcohol. The resulting solution was stirred for 72 h at room temperature to obtain a homogeneous sol. The slow evaporation (50 °C) of solvent produced a violet transparent gel, which was dried in oven (120 ^oC, 24 h) to obtain X-ray amorphous xerogel. The xerogel was grounded and heated in a laboratory furnace at 300 ^oC to burn out the organic residues and calcined at higher temperature (400-1200 ^oC) to obtain nanocrystalline $CoGa_2O_4$ with different average particle sizes. $CoGa_2O_4$ powder was also synthesized by complexing Co^{2+} and Ga^{3+} ions in an ethylene glycol solutions.[23] After the slow evaporation of glycol (< 100 ^oC), the resinous mass obtained was calcined and heat-treated at 1000 ^oC (6 h).

CVD

A cold-wall horizontal low-pressure CVD reactor was used in this experiment. The substrate (Si) was placed on a graphite susceptor and heated (450-650 ^oC) inductively using a radio frequency generator. Optical pyrometer and a thermocouple were used to monitor the substrate temperature with accurary ± 1 ^oC. The precursor reservoir was maintained at the required temperature (105-140 ^oC) for an adequate flux. The precursor flux was regulated from the feedback of the pressure measurement in the reactor during the CVD process. The thermolysis products and unreacted precursor were removed through the pumping. A

quadrupole mass spectrometer was connected to the quartz tube to provide an on-line analysis of the decomposed fragments of the precursor.

Characterization

For studying the decomposition pathway of the precursor, the xerogel was placed in a TGA/DTA crucible, and heated upto 1200 °C, with a ramping rate of 10 ^{o}C/min. The FT-IR spectra of $CoGa_2O_4$ powders were recorded in a KBr matrix on a Biorad-165 Fourier Transform spectrometer whereas the spectrum of $CoGa_2O_4$ film was recorded in reflection mode. XRD data of $CoGa_2O_4$ powders were collected with a STOE diffractometer (STADIP) operating with a CuK_α radiation. XRD patterns of $CoGa_2O_4$ films were recorded on an Siemens D-500 diffractometer with small incident angle (~ 1°). XRD data were used to calculate the average sizes of $CoGa_2O_4$ nanoparticles using Scherrer's formula. Particle morphology and elemental distribution in xerogel and calcined powders were recorded using a scanning electron microscope JSM-6400F (JEOL) coupled with an Energy Dispersive X-ray (EDX) facility. TEM analyses were performed by drawing an amorphous carbon coated copper grid through sonicated dispersions ($Pr^{i}OH$) of the samples derived from alkoxide and glycolate routes. The film surface topology and average roughness were analyzed with a Topometrix TMX2000 Explorer atomic force microscope (AFM) using a Si_3N_4 standard tip (radius, 20 nm). The UV-Vis spectra of $CoGa_2O_4$ powders were recorded with the help of an integrating sphere by Cary 5E UV-Vis spectrometer. Magnetic measurements on nanopowder samples were accomplished using a commercial SQUID magnetometer at room temperature and applied fields up to 20 kOe.

Results and discussion

Synthesis and Processings

The hetero-bimetallic precursor, $[CoGa_2(OBu^{t})_8]$, was obtained by a salt-elimination reaction between anhydrous cobalt chloride and sodium *tetra*-alkoxogallate as reported by

Singh and Mehrotra.[19] The crystals of $[CoGa_2(OBu^t)_8]$ were found to be unsuitable for single crystal X-ray diffraction analysis. The product crystallized from a concentrated toluene solution produced crystals of poor quality, most of them were twinned and degraded catastrophically during the X-ray diffraction analysis (several crystals were examined). The powder X-ray diffraction studies were prevented by extremely hygroscopic nature of the crystals, which made sample preparation (filling the powdered samples in glass capillary) difficult as the product upon pulverization formed a wax-like mass. Elemental analysis in $[CoGa_2(O^tBu)_8]$ was performed gravimetrically: (MW: 789 Da): Co 7.38 (found: 7.18); Ga 17.49 (found: 17.88), which provided Co:Ga ratio of 0.96: 2.04 and supported the proposed chemical formula. The proposed chemical composition (Scheme 1) for the title compound was supported by the elemental analyses as well as the structural data available for similar transition metal aluminates $[MAl_2(OBu^t)_8]$ (M^{II} = Co, Ni, Cu, Fe, Zn)[14,15] and recently reported $[NiGa_2(O^tBu)_8]$.[24] The thermal fragmentation of the precursor during CVD experiment was examined by on-line mass spectroscopy, whereby major products were identified to be H_2O^+, $C_2H_4^+$, $C_3H_6^+$ and $C_4H_8^+$ whose distributions in the gas phase were found to be temperature dependent.[24]

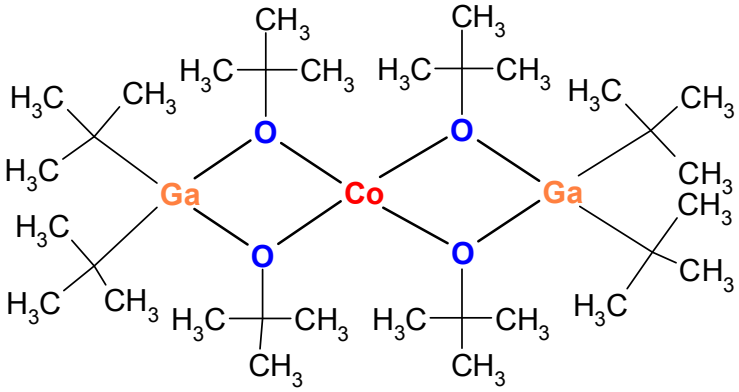

Scheme 1. Proposed molecular structure of $[CoGa_2(O^tBu)_8]$.

Thermal, Phase, Microstructure Analyses

TG-DTA profiles of $[CoGa_2(O^tBu)_8]$ in dry synthetic air (Fig. 1a) showed three distinct steps: (i) in range 20 to 200 °C, evaporation of volatile components takes place, which is indicated by a strong endothermic peak observed at 180 °C and associated with nearly 52 % weight loss. (ii) The strong exothermic peaks at 313, 384 and 432 °C correspond to oxidative expulsion (combustion) of organic ligands. The exothermic peak at 480 °C suggests the incipient crystallization of spinel phase with no significant weight loss observed afterward. The observed gradual weight gain at higher temperature (480 -1200 ^oC) is possibly due to the uptake of oxygen from the surrounding, which indicates either micro-phase separation (Ga_2O_3 and CoO_x), which would increase the metal:oxygen ratio (0.75 for spinel) or formation of non-stoichiometric oxides. The appearance of this feature at rather high temperature indicates that additional oxygen contributing towards weight gain is not originating from the source molecule as the precursor decomposition is already completed below 480 °C and the rest oxygen is eliminated as volatile byproducts. This aspect was not further investigated in this study.

The IR spectra of heat-treated (400 - 1000 °C) $CoGa_2O_4$ powders (Fig. 1b) exhibit the characteristic spectral pattern expected for $CoGa_2O_4$ consisting of two well-defined groups of sharp peaks in the range 300-800 cm^{-1}, which is conform with the reported data.[14] The peaks are more resolved for samples heat-treated at higher temperatures probably due to enhanced crystallinity. When compared to powder samples, the CVD deposit (at 550 ^oC) reveals a shift to large wave number (~ 140 cm^{-1}) indicating the probable presence of stress within the thin film form. Further, the broad band centred at 3400 cm^{-1} can be ascribed to stretches of metal-bound hydroxy groups. The bands corresponding to C-H, C-C and C-O vibrations of the residual alkoxy groups are observed in the regions of lower wave numbers. The absence of peaks characteristic of C-H fragements despite lower deposition temperature (550 ^oC) indicates an effective ligand-stripping in the gas phase decomposition of $[CoGa_2(O^tBu)_8]$.

The phase composition of spinel powders calcined at 400 and 600 °C revealed poor crystallinity, however the major peaks at 36 and 63° (Fig. 2) could be assigned to $CoGa_2O_4$ phase (PDF [11-0698]). At 800 °C and above, the FWHM of the XRD peaks become narrower indicating the grain growth in the samples (Fig. 2a). Figure 2b shows XRD-patterns of $CoGa_2O_4$ films deposited at different substrate temperatures (450 - 650 °C); the film deposited at 450 °C is amorphous whereas crystalline $CoGa_2O_4$ phase is already obtained at 550 and 650 °C.

To evaluate the particle size and chemical homogeneity in $CoGa_2O_4$ phases synthesized by molecular and glycolate approaches, transmission electron microscopy (Fig. 3) was performed in both the cases. The sample obtained from glycolate synthesis (Fig. 3a) revealed strong agglomeration of particles with diameter ranges lying in tens to several hundreds of nanometers. The particles obtained from gycolate route show irregular form composed of amorphous and crystalline parts which were evident in HR-TEM image (Fig. 3c). The TEM image (Fig. 3b) of the alkoxide-derived sample (calcined at 1000 °C) showed regularly dispersed crystallites of nearly uniform size (~ 100 nm). The distinct lattice fringes observed in HRTEM image (Fig. 3d) confirmed the high crystallinity and phase purity of $CoGa_2O_4$ nanoparticles.

In-plane and cross-sectional SEM images of CVD film deposited on Si substrates (Fig. 4a) at 550 °C typically showed the compact coating with granular morphology, which can be attributed either to the lattice mismatch between film and substrate to competitive 2D (films) and 3D (islands) growth mechanisms due to different interfacial/surface energies. The cross-sectional SEM image of $CoGa_2O_4$ film revealed a dense film of homogeneous thickness (Fig. 4a). An EDX line-scan confirmed a homogeneous atomic ratio (Co:Ga ~ 1:2) across the film. The homogeneity of the surface morphology was conformed by AFM analysis which showed the film to be smooth (R_a ~ 50 nm) with no cracks or inhomogeneous growth (Fig. 4b).

Optical and Magnetic Properties

The UV-Vis spectra (Fig. 5) of sol-gel derived $CoGa_2O_4$ powders show the characteristic features of Co^{2+} ions present in the tetrahedral and/or octahedral configurations. A triple band (tetrahedral: $^4A_2(F) \rightarrow {}^4T_1(P)$; octahedral: $^4T_1(F) \rightarrow {}^4T_1(P)$) located at 500-800 nm can be attributed to a John-Teller distortion of the Co^{2+} in the crystal field.[25-27] The color of $CoGa_2O_4$ powders changed from dark-green (400 - 500 ^oC) to grass green (600 - 800 ^oC) and finally to blue (1000 - 1200 ^oC). The peaks I, II and III located at 560, 600 and 650 nm, can be considered as the spectral distribution of green, yellow orange and red colors, respectively. The peaks I and II reveal an increase in intensity with respect to peak III upon increasing the calcined temperature. Peaks II and III shift to low wavelength whereas the peak I is fixed. Previous investigation[15] on $ZnAl_2O_4$ has shown that it has a partially inverse structure at low crystallization temperature, which was confimed by the co-existence of 4- and 6-fold coordinated Al centers by 27Al solid state NMR analysis.[15] The degree of inversion is reduced upon heat-treatment at high temperatures, which result in the thermodynamically controlled migration of Al ions from tetrahedral into octahedral sites. This is evident in the gradual decrease of the NMR peaks corresponding to AlO_4 units.[15] The evoluation of inverse/normal conversion of $CoGa_2O_4$ can be reflected in the change of Co^{2+} triple band (Fig. 5). The triple band of $CoGa_2O_4$ calcined at lower temperatures (400 - 600 ^oC) can be considered as the summation of contribution from inverse and normal spinel phases.

Since the Co^{2+} ion is the only magnetic ion in the $CoGa_2O_4$ compound which can be distributed in tetrahedral (A) and octahedral (B) sites, the magnetization is composed of A-A, B-B and A-B magnetic interactions among Co^{2+} ions. D. Fiorani et al.[28] have reported that the polycrystalline $CoGa_2O_4$ revealed an antiferromagnetic order with $T_N \sim 10$ K. Figure 6 shows the room temperature M-H curve of $CoGa_2O_4$ nanopowder (1000 ^oC) which indicated the typical antiferromagnetic behaviour in the nanocrystalline $CoGa_2O_4$. The influence of size

effect on the magnetic and spin-glass behaviours of nanocrystalline $CoGa_2O_4$ films and particles at low temperature is currently being investigated.

Conclusions

This report describes the decomposition behaviour of a molecular precursor $[CoGa_2(O^tBu)_8]$ containing –Co–O–Ga– units and cation ratio (Co:Ga = 1:2) enabling a low temperature synthesis of $CoGa_2O_4$ spinel. The chemical composition (EDX) and structural (FT-IR, XRD, SEM and TEM analyses) indicated that monophasic $CoGa_2O_4$ can be easily obtained in film and particle forms following molecule-based growth. Application of well-defined molecules as precursor units offers precise control over structure, morphology and composition of resulting nanomaterials either through intrinsic influence of chemical design or by easier variation of process parameters, which enables the tuning of phase and morphology in the resulting material (Scheme 2).

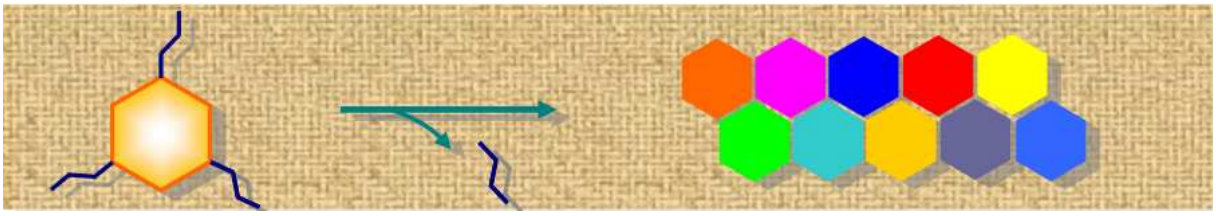

Scheme 2. Controllable transformation from molecule to materials.

Acknowledgement

Thanks are due to the German Science Foundation (DFG), Federal Ministry of Education and Research (BMBF) and University of Cologne for supporting this work.

References

1. M. Z.Wu, Y. D. Zhang, and S. Hui, *J. Appl. Phys.,* 2002, **92**, 6809.

2. D. Michels, C. E. Krill, and R. Birringer, *J. Magn. Magn. Mater.*, 2002, **250**, 203.

3. K. V. P. M. Shafi, A. Ulman, and A. Dyal, *Chem. Mater.*, 2002, **14**, 1778.

4. C. Binns, S. H. Baker, and M. J. Maher, *Phys. Status. Solidi. A*, 2002, **189**, 339.

5. J. D. Ye, K. Chen, and A. Dominguez-Rodriguez, *J. Inorg. Mater.*, 1998, **13**, 257.

6. S. Wojciechowski, J. Mater. Process. Tech., 2000, **106**, 230.

7. R. J. Gehr, and R.W. Boyd, *Chem. Mater*., 1996, **8**, 1807.

8. R. Van de Krol, and H. L. Tuller, *Solid State Ionics*, 2002, **150**, 167.

9. H. Gleiter, *Acta Mater*., 2000, **48**, 1.

10. A. P. Alivistos, *Science*, 1996, **271**, 933.

11. J. H. Fendler, (Ed.), *Nanoparticles and Nanostructured Films,* Wiley-Vch, Germany, 1998.

12. A. Wiedenmannn, U. Lembke, A. Hoell, *Nanostruct. Mater*., 1999, **12**, 601.

13. (a) S. Mathur and H. Shen in *Encyclopedia of Nanoscience and Nanotechnology*, Ed. H. Nalwa, American Scientific Publisher, 2004, **4**, 131. (b) S. Mathur, *Chemical Physics of Thin Film Deposition – Processes for Micro- and Nano-Technologies*, 2002, 91.(c) H. Shen and S. Mathur, *J. Phys. IV France*, 2002, **12**, Pr 4-1. (d) M. Veith, S. Mathur, C. Mathur, *Polyhedron*, 1998, **17**, 1005. (e) S. Mathur, M. Veith, H. Shen, S. Hüfner, and M. Jillavi, *Chem. Mater.,* 2002, **14**, 568. (f) M. Veith, S. Mathur, H. Shen, N. Lecerf, S. Hüfner, and M. Jillavi, *Chem. Mater.,* 2001, **13**, 4041. (g) S. Mathur, H. Shen, N. Lecerf, A. Kjekshus, H. Fjellvag and G. F. Goya, *Adv. Mater.,* 2002, **14**, 1405. (h) M. Veith, S. Mathur, N. Lecerf, H. Shen, and S. Hüfner, *Chem. Mater.,* 1999, **11**, 3103. (i) S. Mathur, M. Veith, V. Sivakov, H. Shen, V. Huch, U. Hartmann, H. B. Gao, *Chem. Vap. Deposition*, 2002, **8**, 277. (j) S. Mathur, M. Veith, T. Ruegamer, E. Hemmer, and H. Shen, *Chem. Mater*., 2004, **16**, 1304. (k) S. Mathur, M. Veith, R. Rapalaviciute, H. Shen, G. F. Goya, W. L. Martins Filho, and T. S. Berquo, *Chem. Mater.,* 2004, **16**, 1906. (l) S. Mathur, H. Shen, V. Sivakov and U. Werner, *Chem. Mater*., 2004, **16**, 2449.

14. F. Meyer, R. Hempelmann, S. Mathur, M. Veith, *J. Mater. Chem*., 1999, **9**, 1755.

15. S. Mathur, M. Veith, M. Haas, H. Shen, N. Lecerf, V. Huch, S. Hüfner, R. Haberkorn, H. P. Beck, M. Jilavi, *J. Am. Chem. Soc*., 2001, **84**, 1921.

16. I. K. Jeong, H. L. Park, S.-I. Mho*, Solid State Com.*, 1998, **105***,* 179.

17. S. Daniele, D. Tcheboukov, L. G. H. Pfalzgraf, *J. Mater. Chem*., 2002, **12***,* 2519.

18. P. D. Rack, J. J. Peterson, M. D. Potter, W. Park, *J. Mater. Res*., 2001, **16***,* 1429.

19. (a) R. C. Mehrotra, J. Singh, *Can. J. Chem*., 1984, **62***,* 1003. (b) R. C. Mehrotra and J. V. Singh*, Z. Anorg. Allg. Chem.* 1984, **512***,* 221.

20. J. L. Soubeyroux, D. Fiorani and E. Agostinelli, *J. Mag. Mag. Mater.,* 1986, **54**, 83.

21. U. Bhattacharya and V. S. Darshane, *J. Mater. Chem*., 1993, **3**, 299.

22. M. Veith, S. Mathur and V. Huch, *J. Am. Chem. Soc.* 1996**, 118**, 903.

23. M. Veith, S. Mathur, A. Kareiva, M. Jilavi, M. Zimmer and V. Huch, *J. Mater. Chem.,* 1999, **9***,* 3069.

24. S. Mathur, S. Barth and H. Shen, *Chem. Vap. Deposition*, 2005, **11**,11.

25. J. S. Griffith, *The Theory of Transition-Metal Ions*, Cambridge University Press, London, 1971.

26. U. L. Stangar and B. Orel, *J. Sol-Gel Sci. Techn.*, 2003, **26**, 771.

27. M. Zayat and D. Levy, *Chem. Mater*., 2000, **12**, 2763.

28. D. Fiorani and S. Viticoli, *Solid State Commun*., 1978, **25**, 155.

Figure Captions

Fig. 1. (a) TG/DTA curves of [$CoGa_2(O^tBu)_8$] precursor obtained under synthetic air flow (75 sccm) and 10 ^oC/min ramping rate. (b) FT-IR spectra of $CoGa_2O_4$ samples derived from sol-gel (400, 600, 800 and 1000 ^oC) and CVD (550 ^oC) processes.

Fig. 2. XRD patterns of (a) sol-gel derived $CoGa_2O_4$ samples calcined at 400, 600, 800 and 1000 ^oC and (b) $CoGa_2O_4$ films deposited at 450, 550 and 650 °C.

Fig. 3. TEM images of $CoGa_2O_4$ nanopowders (1000 ^oC) obtained from (a) glycolate and (c) alkoxide routes. The corresponding HR-EM images are shown in (b) and (d).

Fig. 4. (a) In-plane and cross-sectional SEM and (b) AFM images of $CoGa_2O_4$ film deposited at 550 ^oC.

Fig. 5. UV-VIS spectra of sol-gel derived $CoGa_2O_4$ samples calcined at 400, 500, 600, 800 and 1200 ^oC.

Fig. 6. Room-temperature M-H curve of $CoGa_2O_4$ sample calcined at 1000 ^oC.

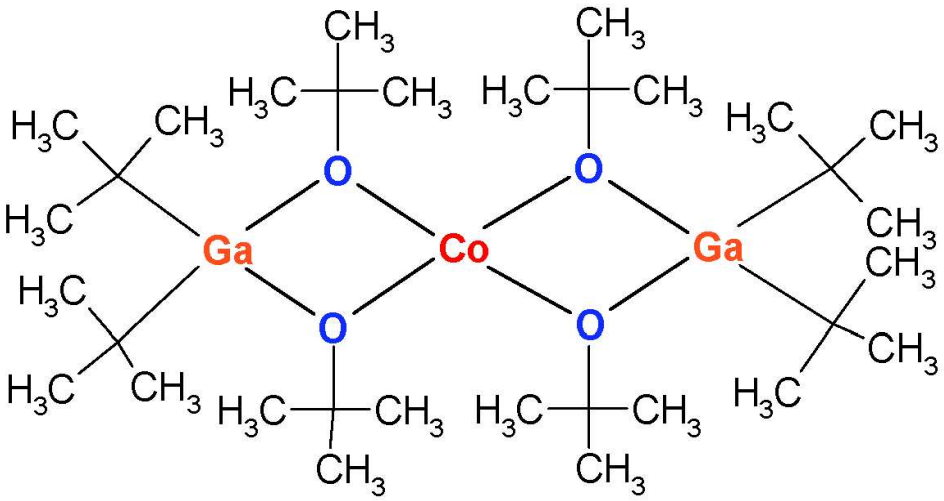

Scheme 1
103x55mm (300 x 300 DPI)

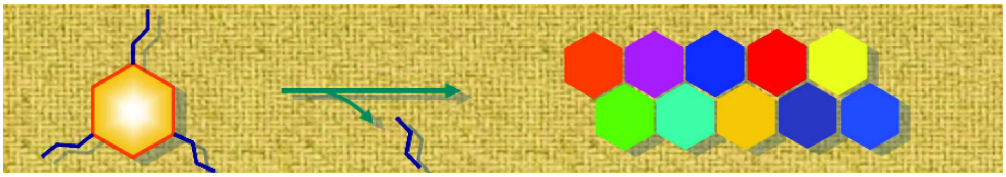

Scheme 2
159x26mm (300 x 300 DPI)

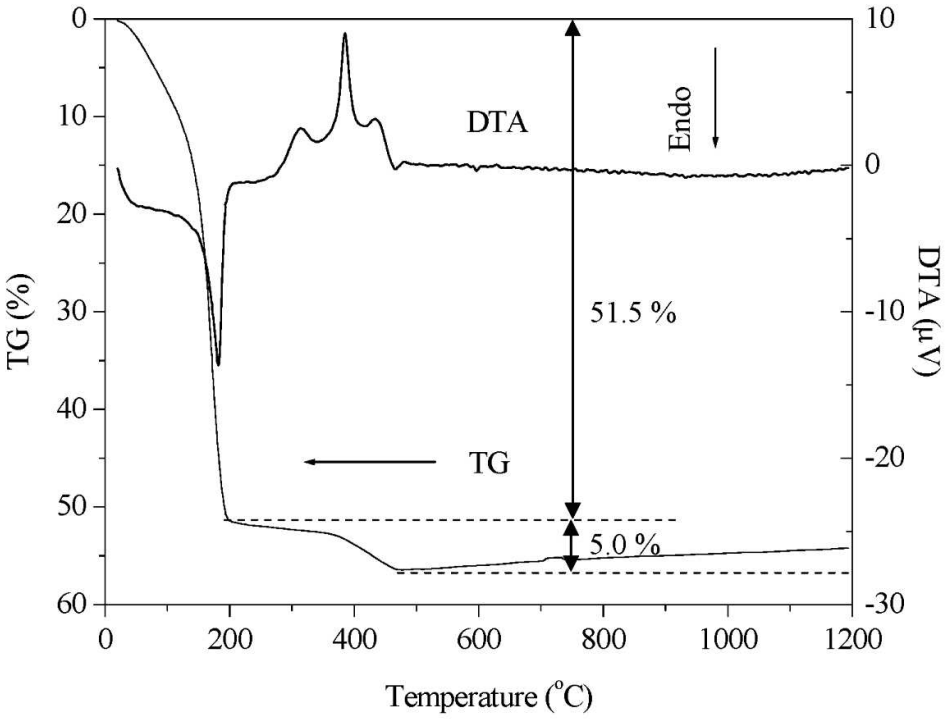

Figure 1a
103x75mm (300 x 300 DPI)

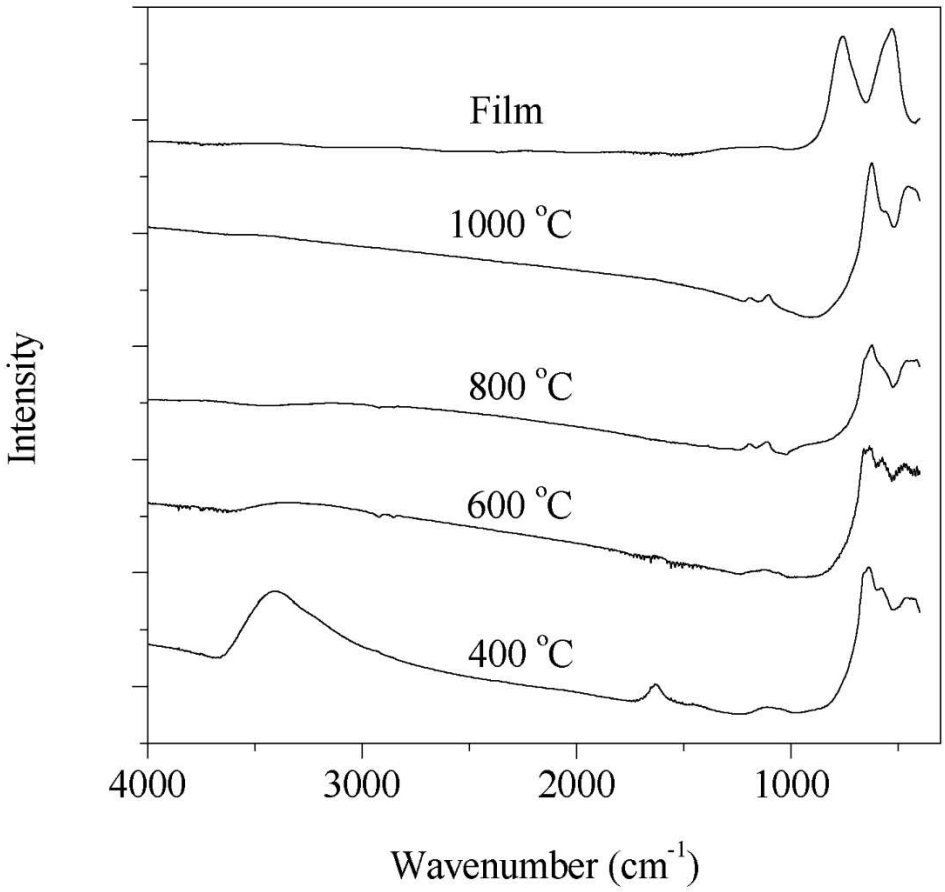

Figure 1b
97x90mm (300 x 300 DPI)

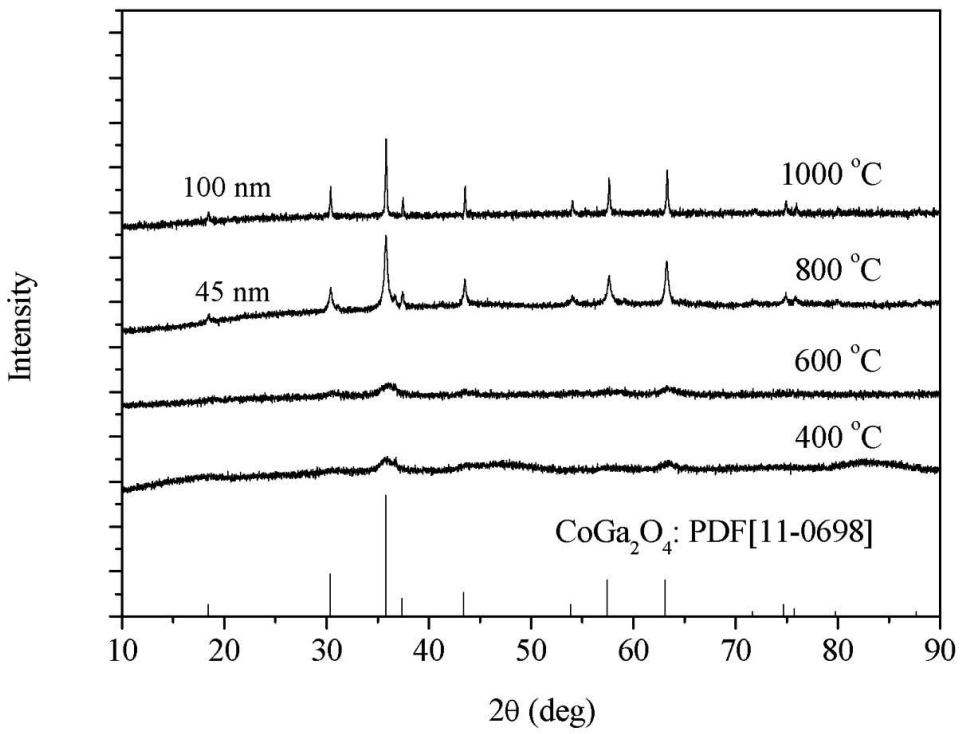

Figure 2a
106x82mm (300 x 300 DPI)

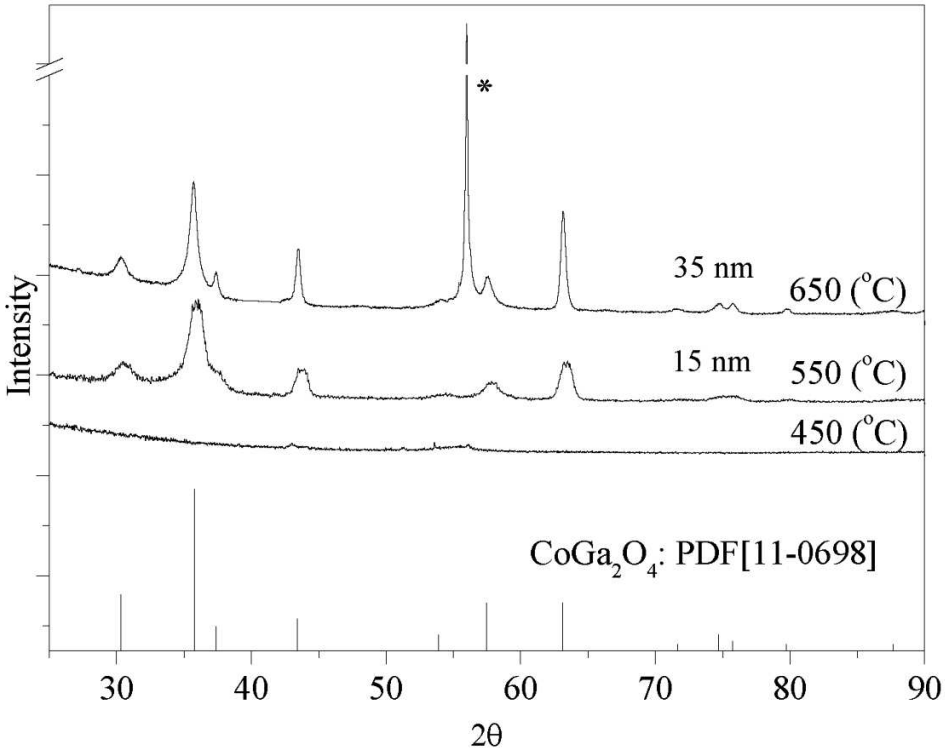

Figure 2b
99x79mm (300 x 300 DPI)

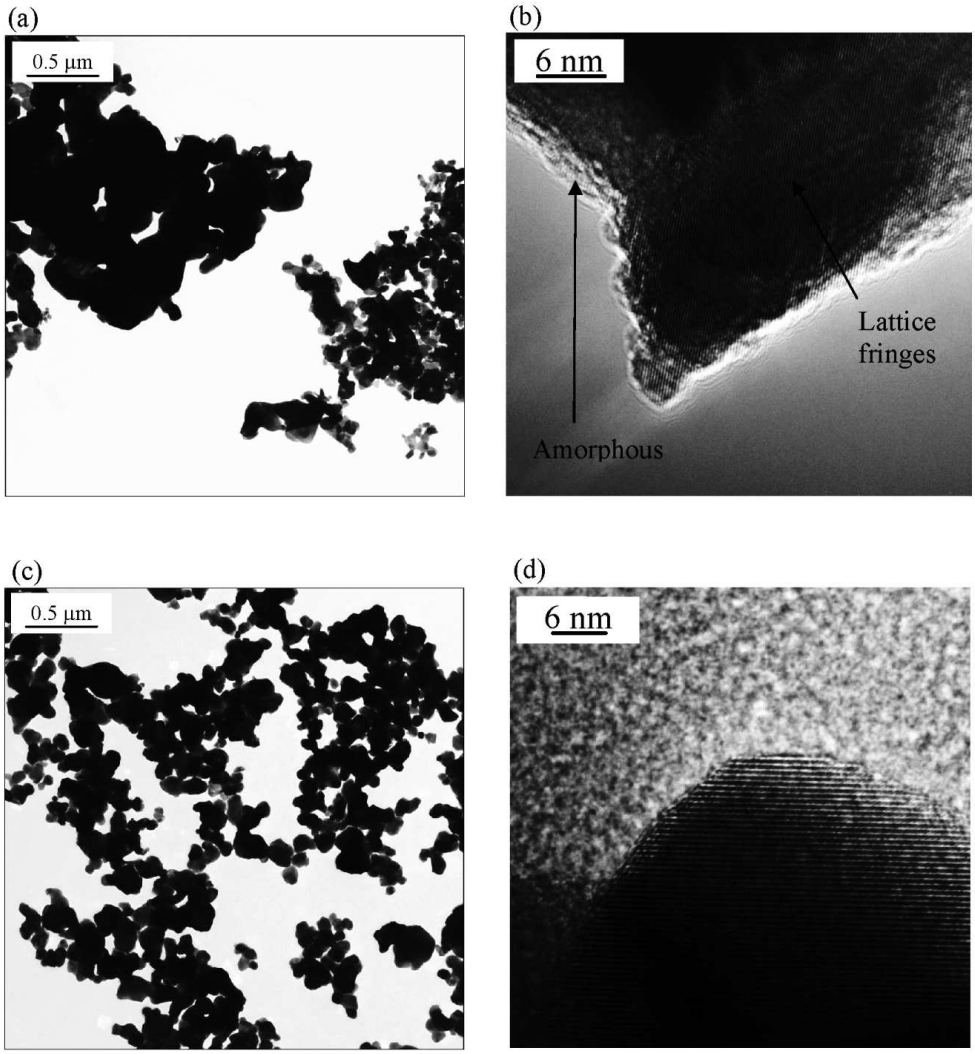

Figure 3
114x123mm (300 x 300 DPI)

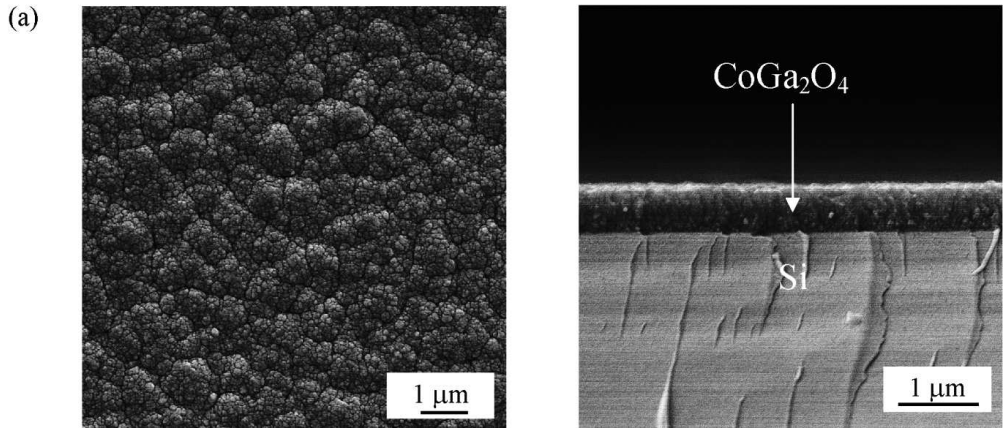

Figure 4a
115x51mm (300 x 300 DPI)

(b)

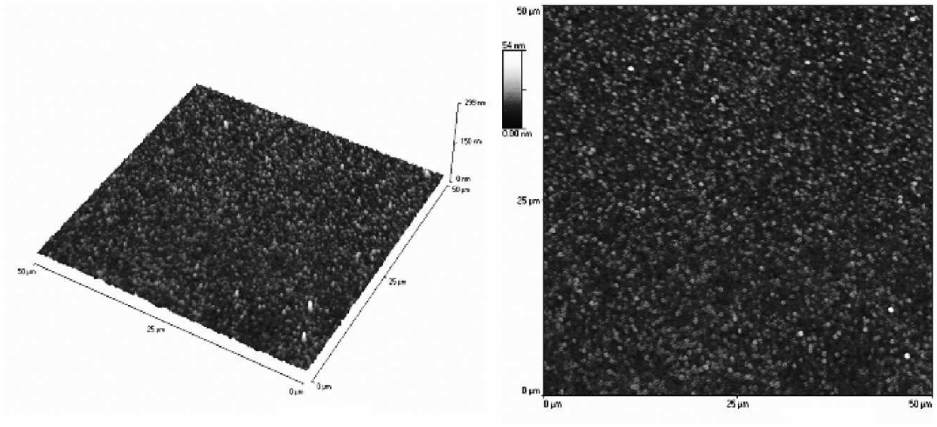

Figure 4b
119x65mm (300 x 300 DPI)

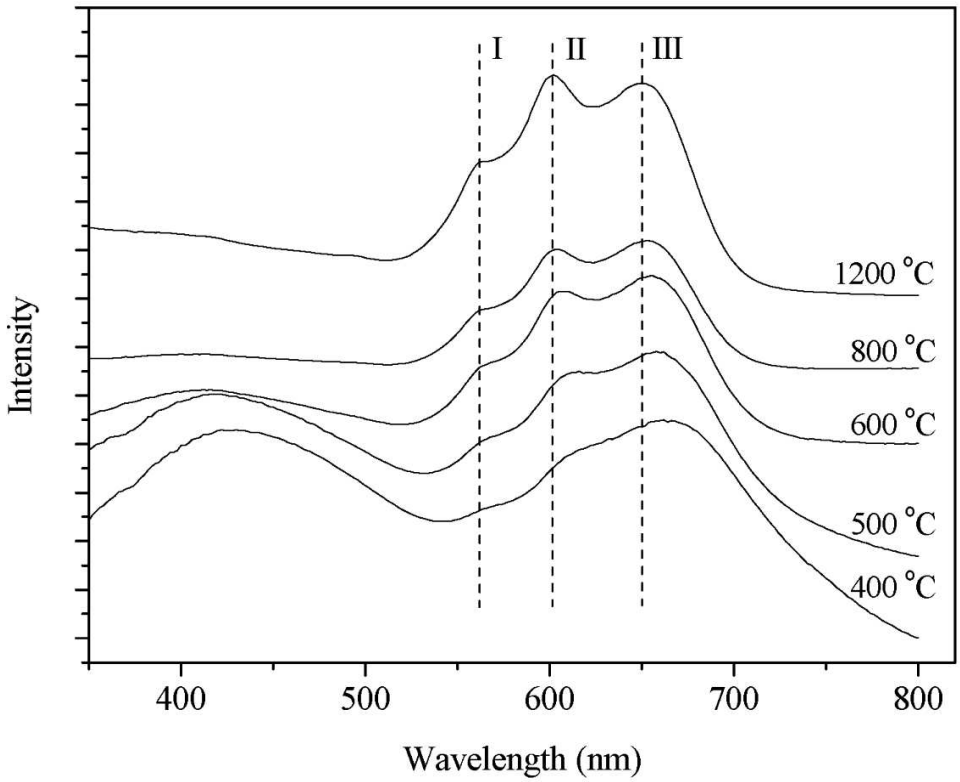

Figure 5
99x81mm (300 x 300 DPI)

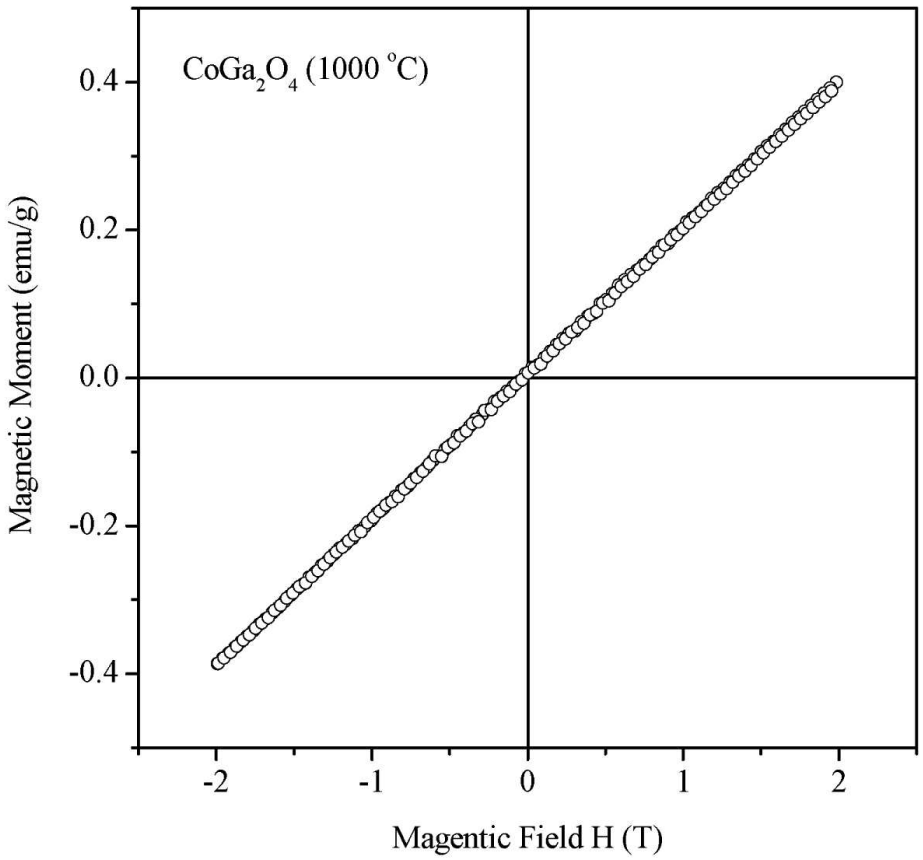

Image 6
108x98mm (300 x 300 DPI)